Design of a creep resistant nickel base superalloy for power plant applications Part 2—Phase diagram and segregation simulation

F. Tancret and H. K. D. H. Bhadeshia

Models have been developed and used as tools to design a new 'made to measure' nickel base superalloy for power plant applications. In Part 1 Gaussian processes were used to model the mechanical properties of superalloys, and have been used as a basis for the design of a new Ni–Cr–W–Al–Ti–Fe–Si–C–B superalloy with desirable properties. In this part, an attempt has been made to design against the formation of undesirable phases, and to calculate the solidification range, forging window and heat treatment, using phase diagram calculations. The potential for chemical segregation has also been estimated following Scheil's assumptions, and remains acceptable. MST/5390

Dr Tancret is in the Laboratoire Génie des Matériaux, Polytech' Nantes, La Chantrerie – Rue Christian Pauc, BP 50609, 44306 Nantes Cedex 3, France (franck.tancret@polytech.univ-nantes.fr). Professor Bhadeshia is in the Department of Materials Science and Metallurgy, University of Cambridge, Pembroke Street, Cambridge CB2 3QZ, UK. *Manuscript received 29 January 2002; accepted 18 September 2002.*

Introduction

In Part 1 of this series, a new Ni–20Cr–3·5W–2·3Al–2·1Ti–5Fe–0·4Si–0·07C–0·005B (wt-%) nickel base superalloy has been proposed, for use in future fossil fuel power plant, to operate with steam temperatures as high as 750°C. This alloy has been designed on the basis of its estimated mechanical properties, which have been modelled using a Gaussian processes non-linear multiparameter method. Also, a huge price reduction has been aimed at by avoiding the use of expensive alloying elements such as Co, Mo, Ta, and Nb. The designed alloy should have a creep rupture life of 100 000 h at 750°C under a stress of 100 MPa.

This alloy should also be forgeable, weldable, oxidation resistant, and its microstructure should be stable over long exposures at service temperature.

However, Gaussian processes models do not take into account any metallurgical knowledge about phase formation and stability. Thus, when used to predict the mechanical properties of a novel alloy, those models perform interpolations or limited extrapolations. Thus, even if the methodology has often proved successful, it may happen that a non-desired phase forms in the novel alloy, which could not be predicted by the mechanical property models, and could be detrimental to the mechanical properties.[1] Also, the occurrence of microsegregation during solidification of a new alloy could have a major influence on its subsequent processability, in particular on its forgeability.

For these reasons, use has been made of a phase diagram and microsegregation computer simulation approach as part of the recent design of this new creep resistant nickel base superalloy for power plant applications, in parallel with the Gaussian processes modelling of mechanical properties presented in Part 1.[2–4]

Modelling procedure

A thermodynamic simulation software, Thermo-Calc,[5] has been used in conjunction with a proprietary nickel base superalloys database developed by Rolls-Royce and Thermotec Ltd. The program uses phase diagram calculations to extrapolate thermodynamic descriptions for use in an n-component system based on the assessment of binary, ternary, and quaternary experimental data. It puts several models to work to minimise the Gibbs free energy of phases in the system, such as the regular solution model and several extensions based on it, e.g. the sublattice model. It can be used to predict the phases present as a function of temperature for a vast range of alloy compositions, and thus to check if undesirable phases, e.g. σ and ν in superalloys, are to be expected or not.

Also, a special module has been written and used to simulate microsegregation during solidification, based on Scheil's approximation. The latter assumes a perfectly homogeneous liquid and a solid without diffusion. Temperature is decreased by small steps (1 K), and at each step a new liquid–solid equilibrium is calculated, the amount and composition of the liquid being kept as inputs for the next step. The total amount of solid is the sum of solid quantities calculated at each step over the whole process. This also allows the evolution of the liquid composition to be followed relative to the nominal alloy composition, and to predict the microsegregation behaviour.

Results and discussion

EQUILIBRIUM PHASE DIAGRAM

The expected equilibrium phases have been calculated using Thermo-Calc over a wide range of temperatures, from the liquid phase down to 500°C, well below the normal service temperature of 750°C. The predictions are reported in Fig. 1 on a three-scale plot of the molar amount of phases versus temperature.

Major phases

On the main scale of Fig. 1 (top scale, 0–100%), the evolution of molar fractions of the principal phases γ, γ', and liquid, has been plotted. The calculated liquidus, solidus, and γ' solvus temperatures are 1381, 1299, and 1011°C, respectively. This is extremely important for fabrication: the alloy should be liquid above 1381°C, solidify between 1381 and 1299°C, and can be forged in the γ' free region between

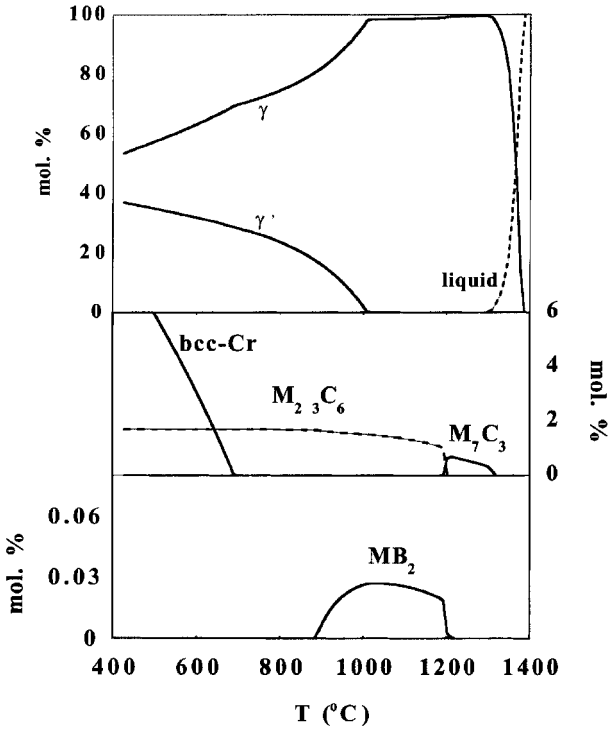

1 Predicted equilibrium phase formation in designed alloy as a function of temperature

the γ' solvus and the solidus, i.e. between 1011°C and 1299°C. However, because chemical segregation often occurs during solidification, the latter is likely to extend to temperatures lower than the calculated equilibrium one,[6,7] which reduces the actual forging window. This particular point will be discussed later. Nevertheless, the calculated forging window of 288 K is wider than in many γ' strengthened commercial superalloys (for example, 159 K in Udimet 500 and 149 K in Inconel 718), and should remain wide enough for forging, even if it is reduced by segregation. This graph also indicates the solution and aging heat treatments ranges, i.e. between 1011°C and 1299°C, and below 1011°C, respectively. Finally, the expected γ' fraction at the service temperature of 750°C is 26 mol.-%, which also matches the criterion of a weldable superalloy.[8]

Carbides and borides

The calculated molar amounts of carbides are presented on the middle scale of Fig. 1. A high temperature 'Cr_7C_3' type carbide phase should be present in the γ' free region, as in some Ni base superalloys. If properly solution heat treated, these carbides should decompose at lower temperatures into $M_{23}C_6$ carbides ('M' being mainly chromium) and precipitate at γ grain boundaries. Care should be taken during heat treatment to ensure fine grain boundary $M_{23}C_6$ particles and not a continuous film. Indeed, if the former kind is beneficial for creep resistance in preventing the grain boundary sliding mechanism, the latter is detrimental since it favours the propagation of large creep cracks.[9]

On the bottom scale of Fig. 1, it can be seen that 'TiB_2' type borides are expected to form between 885°C and 1226°C, and to dissolve at lower temperatures. However, this results from equilibrium calculations, which do not take grain boundaries into account. Indeed, boron segregates at grain boundaries.[10] Consequently, the formation of borides will have to be checked experimentally in the alloy produced.

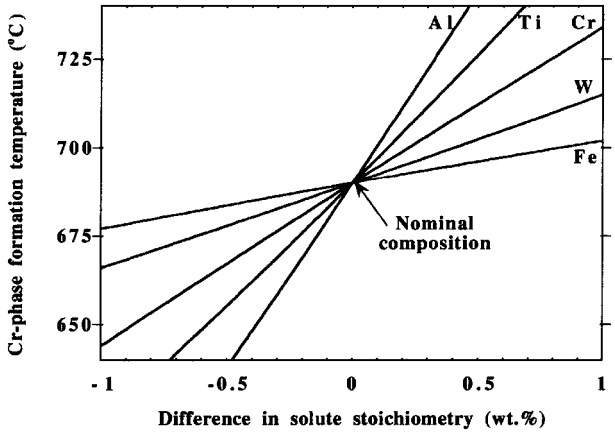

2 Predicted equilibrium formation temperature of α-Cr phase in designed alloy when Al, Ti, Cr, W, or Fe content is varied around nominal composition

UNDESIRABLE PHASES

On the middle scale of Fig. 1, it can be seen that, under equilibrium conditions, a body centred cubic α-Cr phase is predicted to form below 690°C. This phase, even if similarly predicted in some chromium rich commercial nickel base superalloys, e.g. Nimonic 81, has not been reported to form. Consequently, its influence on the mechanical properties of such materials is unknown. However, the α-Cr phase is quite common in chromium rich NiAl and Ni_3Al intermetallic based alloys,[11,12] and has been found to form at high temperatures (>900°C) in the γ' phase after nucleating from γ. Thus, it is possible that this phase also forms in Cr rich Ni base superalloys with a γ/γ' microstructure, in a different temperature range.[13] Nevertheless, the calculated formation temperature range of this α-Cr phase in the designed alloy is below 690°C, well below the expected service temperature, and the associated kinetics might be very slow (especially because it is the growth of a bcc phase within a fcc phase), which is probably why it has not been reported in the literature.

The formation temperature of this phase is influenced by alloy composition (Fig. 2). Increasing the Cr content enables the solubility limit of Cr in γ to be reached at higher temperatures. W and Fe, because they both partition partly to γ and substitute for Ni in the same way that Cr does, decrease the solubility of Cr in γ and favour the precipitation of the α-Cr phase at higher temperatures. The role of Al and Ti is different, since they both mainly partition to γ' by forming the $Ni_3(Al,Ti)$ intermetallic phase. Thus, adding one Al or Ti atom takes three Ni atoms from the matrix, which decreases the total amount of γ, increases the Cr concentration in it, and favours the precipitation of the α-Cr phase. This is very important because composition tolerances are necessary for industrial processing: taking the usual tolerances for Cr, W, Al, Ti, and Fe, and setting them at their maximum values raises the formation temperature of the α-Cr phase to 750°C, which is the service temperature. This is the reason why, in Part 1, W, Al, and Ti contents have been kept as low as possible such that the mean creep rupture stress prediction matches the target, and not the lower bound. The present alloy design is thus a well balanced compromise between mechanical properties and phase stability.

Finally, and this is one of the most important points, no other undesirable phases are expected to form in the vicinity of the service temperature. Phases like σ, η, or ν are detrimental to high temperature mechanical properties, in particular creep resistance.[14] Consequently, this alloy compares favourably with other commercial superalloys such as Inconel 718 or Udimet 500, in which such phases have been predicted to form.

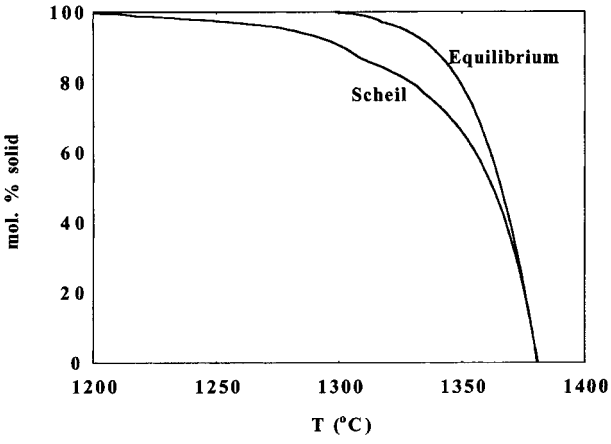

3 Predicted total molar solid fraction as a function of temperature during solidification of designed alloy, calculated under equilibrium or using Scheil's conditions

MICROSEGREGATION

Solidification range

The evolution of solid phase fraction during solidification, studied using Thermo-Calc with both equilibrium data and Scheil's approximation, is presented on Fig. 3 as a function of temperature. Scheil's model assumes a perfectly homogeneous liquid, and that no diffusion occurs within the solid, which may not be true at such high temperatures. Consequently, because back diffusion reduces microsegregation, the actual concentration profile is likely to be between those predicted assuming equilibrium and by the Scheil method.[6,7] A reduction of about 100 K of the forging window can be expected (Fig. 3), the latter probably remaining around 200 K, which is sufficient for safe processing.

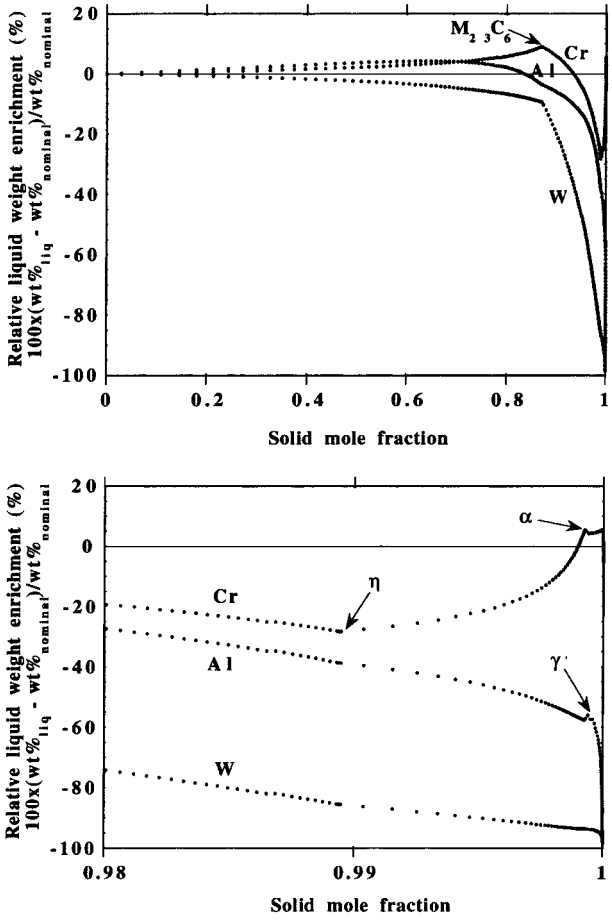

4 Evolution of Cr, W, and Al relative concentrations in liquid as solidification progresses, calculated using Scheil's model

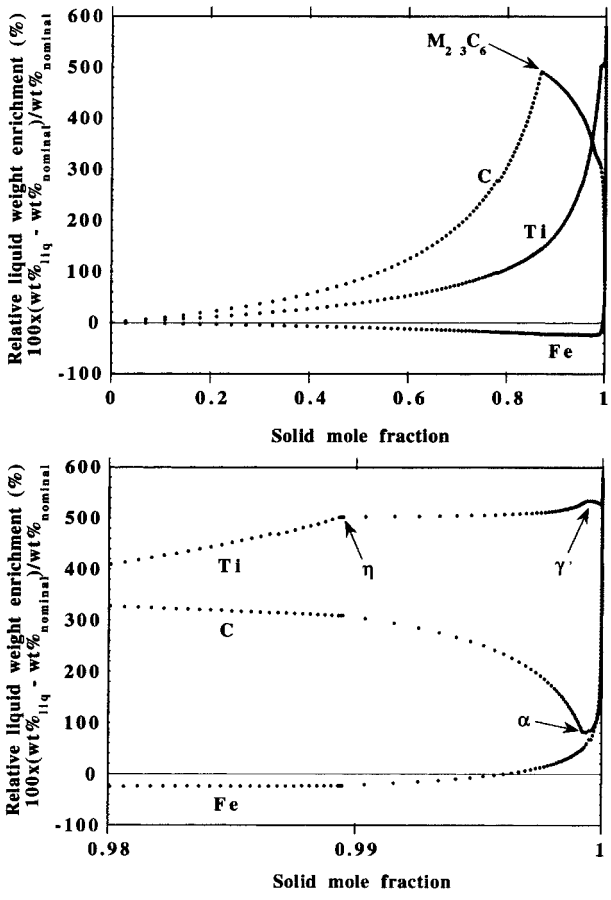

5 Evolution of Fe, Ti, and C relative concentrations in liquid as solidification progresses, calculated using Scheil's model

Phase formation and elemental segregation

Figures 4, 5, and 6 present the evolution of the concentration of various elements in the liquid as a function of the total solid fraction, normalised with respect to the nominal composition. Following these concentrations during the solidification simulation allows one to predict which elements will segregate between dendrites; the program also predicts which phases will form as solidification progresses.

The concentrations of Cr and W in the liquid remain within $\pm 10\%$ of the nominal composition until 87% of the material is solidified (Fig. 4). Then Cr and W are removed from the liquid to form $M_{23}C_6$, which will constitute a form of desired segregation, as this carbide is expected in the equilibrium phase diagram of Fig. 1. $M_{23}C_6$ forms below 1309°C, instead of 1204°C at equilibrium. 'M' in $M_{23}C_6$ is mainly Cr, with also several per cent of W, Ni, and Fe, varying throughout solidification.

Aluminium first slightly segregates in the liquid, and then starts to be removed from the liquid around ~70% solid (Fig. 4), as its solubility becomes higher in γ than in the liquid below ~1350°C.

At a higher solid fraction (0·99, ~1217°C), η precipitates, which corresponds to an increase of the Cr concentration in the liquid (Fig. 4). It must be noted that this undesirable phase is expected to form when only 1% of the liquid is left. It should thus represent a very small quantity, especially if one remembers that Scheil's model is the worst possible case. Finally, α precipitates at 1178°C (690°C at equilibrium)

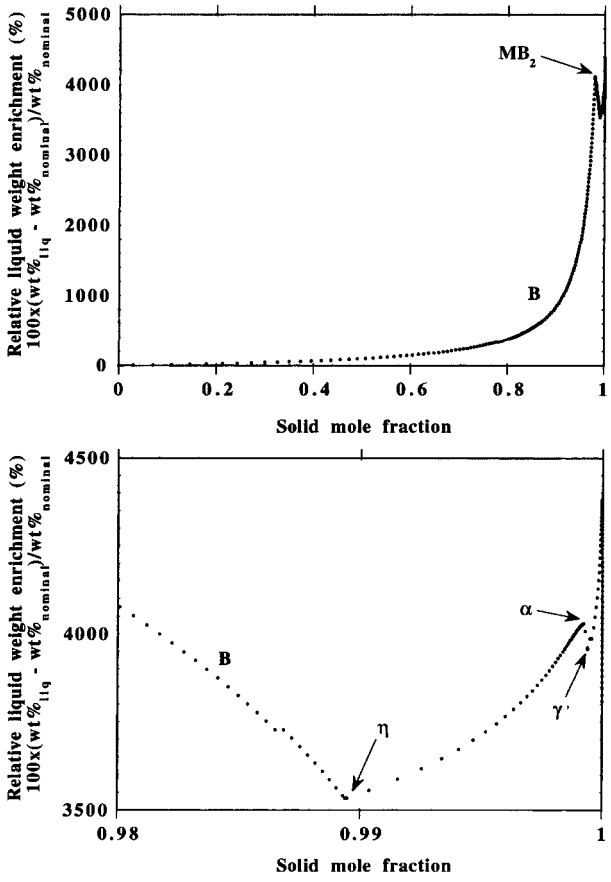

6 Evolution of B relative concentration in liquid as solidification progresses, calculated using Scheil's model

and, apparently, the 'equilibrium' between this nearly pure α-Cr phase and the liquid stabilises the Cr concentration in the liquid until the end of solidification.

Iron behaves differently, as it first slightly concentrates in the solid until solidification is 99·6% complete, and then strongly concentrates in the liquid to reach several times its nominal concentration (Fig. 5). Moreover, the shape of its curve seems not to be affected by the onset of precipitation of other phases (carbides, borides, η, α, γ').

Titanium progressively concentrates in the liquid up to five times its initial concentration (Fig. 5), as its solubility in both γ and $M_{23}C_6$ remains low. The shape of the curve is then slightly affected by the precipitation of η. It finally forms γ' below 1176°C (1011°C at equilibrium).

Carbon segregates to the liquid until $M_{23}C_6$ precipitates (Fig. 5). Then, when α-Cr forms, Cr goes preferentially into α instead of $M_{23}C_6$, and C reconcentrates in the liquid.

Boron strongly segregates to the liquid (Fig. 6), and its concentration reaches almost 45 times that of the nominal composition (which is still only a fraction of a wt-%). It is then partly removed by the precipitation of MB_2 borides below 1241°C (1226°C at equilibrium), but its concentration in the liquid remains high until complete solidification, being modified by the formation of η, α, and γ'. The segregation of boron is not a problem, because, being a small atom, it is likely to diffuse rapidly during heat treatment, but also because boron is intended to be segregated at grain boundaries.

Processing

The usual industrial manufacturing procedure includes casting, remelting, forging, and heat treatment. It has to be designed with respect to the alloy composition and properties, depending on the problems they might cause.

VACUUM INDUCTION MELTING (VIM)

Proper stirring must be ensured when melting W containing alloys, to allow its complete dissolution in the liquid. Tungsten is dense and has a high melting point, and so tungsten particles may just sink in the liquid without dissolving. This problem is common for alloys with high W contents, but our industrial partners advise that it should not occur for the proposed alloy (3·5 wt-%W).

Titanium may pose a problem since it combines with residual nitrogen and oxygen and can remain as inclusions. This should not occur in the novel alloy: when aluminium is present, it combines more strongly with N and O than Ti, but the particles formed float on the liquid and can easily be removed.

ELECTROSLAG REMELTING (ESR)

Casting is usually made as an electrode for arc remelting. The ESR step is not necessary when the first cast is 'perfect', i.e. without macrosegregation, cracks, etc., which is usually the case for small castings, typically $<0{\cdot}5$ ton.

HOT WORKING

The material can be forged, rolled or extruded, all done above the γ' solvus. In the case of forging of large ingots ($>0{\cdot}5$ ton), a typical problem results from the rapid cooling of the surface below the γ' solvus between forge passes, causing severe surface cracking. However, this problem should not occur for low weights and for extrusion, since the process is faster.

Conclusions

A phase diagram simulation software, Thermo-Calc, has been used as a tool in the design of a new creep resistant nickel base superalloy for power plant applications, whose mechanical properties had already been predicted by a previously developed Gaussian processes model (Part 1). The thermodynamical software has been used to predict both the equilibrium phase diagram as a function of temperature, and the potential for solidification microsegregation following Scheil's model.

The calculated equilibrium diagram shows that no undesirable phases should form above 690°C, which is essential for long term microstructural stability. Also, this diagram will be extremely useful in the design of the fabrication procedure, as it indicates the liquidus, the solidus, the γ' solvus, and the formation temperatures of carbides and borides. This allows one to determine the melting and solidification ranges, the forging window, and the heat treatments necessary to precipitate secondary phases.

The occurrence of microsegregation during solidification of the designed alloy, predicted using Scheil's model, should not pose any particular problem. Indeed, the forging window should remain around 200 K, which is still higher than the equilibrium forging window of many commercially available γ' strengthened superalloys. Elements first segregating in the liquid, such as Cr, Al, and Ti, do not form undesirable phases until solidification is 99% complete. The 1% remaining is shared between γ, η, α, and γ'. But, because Scheil's model represents the worst case possible, the actual undesirable phases will probably represent a fraction of a per cent of the total material after solidification. Nevertheless, given the equilibrium phase diagram, η should be dissolved during the high temperature solution heat treatment.

Finally, the state of the art of Ni base superalloys industrial processing has been reviewed with respect to the composition of the designed alloy. Because the tungsten content has been kept low, and because aluminium and titanium are both present (but in low amounts), the

designed alloy should be easily castable and forgeable on a normal industrial scale.

Acknowledgements

The authors are grateful to the Engineering and Physical Sciences Research Council for funding this work, and to Alstom Power, Corus, Mitsui Babcock Energy Ltd., Rolls-Royce plc., Special Metals, and the University of Wales, Swansea, for partnership. The authors thank Doctor Roger Reed and Doctor Phillip Carter for their help within the Rolls-Royce University Technology Centre, and Professor Colin Humphreys for all his support in the Technology Foresight Programme.

References

1. T. COOL: PhD thesis, University of Cambridge, UK, 1996.
2. F. TANCRET, H. K. D. H. BHADESHIA and D. J. C. MACKAY: *ISIJ Int.*, 1999, **39**, 1020 – 1026.
3. F. TANCRET, H. K. D. H. BHADESHIA and D. J. C. MACKAY: *Key Eng. Mater.*, 2000, **171 – 174**, 529 – 536.
4. F. TANCRET: in 'Processing for China', 56 – 58; 2000, London, Sterling Publications.
5. Thermo-Calc, The Royal Institute of Technology, Stockholm, Sweden.
6. U. R. KATTNER, W. J. BOETTINGER and S. R. CORIELL: *Z. Metallkd.*, 1996, **87**, 522 – 528.
7. H. E. LIPPARD, C. E. CAMPBELL, T. BJÖRKLIND, U. BORGGREN, P. KELLGREN, V. P. DRAVID and G. B. OLSON: *Metall. Mater. Trans. B*, 1998, **29B**, 205 – 210.
8. K. M. CHANG and A. H. NAHM: in 'Superalloys 718 – metallurgy and applications', (ed. E. A. Loria), 631 – 646; 1989, Warrendale, PA, TMS.
9. A. K. JENA and M. C. CHATURVEDI: *J. Mater. Sci.*, 1984, **19**, 3121 – 3139.
10. R. F. DECKER and J. W. FREEMAN: *Trans. AIME*, 1960, **218**, 277 – 285.
11. W. F. GALE, R. V. NEMANI and J. A. HORTON: *J. Mater. Sci.*, 1996, **31**, 1681 – 1688.
12. R. YANG, J. A. LEAKE and R. W. CAHN: *Philos. Mag. A*, 1992, **65A**, 961 – 980.
13. R. YANG: Private communication to F. Tancret (2000).
14. C. T. SIMS: *J. Met.*, 1966, **18**, 1119 – 1130.